

Evidence on the incompatibility of modern SPH methods and eddy viscosity models for scale-resolved incompressible turbulence

Max Okraschevski^{1,2,†}, Niklas Bürkle¹, Markus Wicker¹, Rainer Koch¹ and Hans-Jörg Bauer¹

¹Institute of Thermal Turbomachinery, Karlsruhe Institute of Technology, Kaiserstraße 12, 76131 Karlsruhe

²Present Affiliation: Institute of Engineering Thermodynamics, German Aerospace Center, 89081 Ulm, Germany; Helmholtz Institute Ulm for Electrochemical Energy Storage, 89081 Ulm

(Received xx; revised xx; accepted xx)

In this work, we will present evidence for the incompatibility of modern SPH methods and eddy viscosity models. Taking a coarse-graining perspective, we physically argue that modern SPH methods operate intrinsically as Lagrangian Large Eddy Simulations for turbulent flows with strongly overlapping discretization elements. However, these overlapping elements in combination with numerical errors cause a significant amount of implicit subfilter stresses (SFS). Considering a Taylor-Green flow at $Re = 10^4$, the SFS will be shown to be relevant where turbulent fluctuations are created, explaining why turbulent flows are challenging even for modern SPH methods. Although one might hope to mitigate the implicit SFS using eddy viscosity models, we show a degradation of the turbulent transition process, which is rooted in the non-locality of these methods.

1. Motivation

The Smoothed Particle Hydrodynamics (SPH) method was proposed in 1977 as a Lagrangian discretization method for fluid dynamics (Lucy 1977; Gingold & Monaghan 1977) and matured significantly since then as detailed in several reviews (Springel 2010; Price 2012; Monaghan 2012; Shadloo *et al.* 2016; Ye *et al.* 2019; Lind *et al.* 2020; Sigalotti *et al.* 2021). Originally, it features serious numerical convergence problems due to the fact that the consistency of spatial derivative operators is strongly affected by the local particle arrangement, which only can be compensated by a drastic increase in the number of neighbor particles N_{ngb} (Zhu *et al.* 2015). This is especially problematic in strong shear flows and subsonic turbulence, resulting in zeroth-order errors related to excessive numerical dissipation for small N_{ngb} (Ellero *et al.* 2010; Bauer & Springel 2012; Colagrossi *et al.* 2013; Hopkins 2015).

Pioneered by the work of Vila (1999), modern SPH methods, as recently compared by Eirís *et al.* (2023), mostly eliminated this convergence issue by the usage of at least one of the following two strategies

† Email address for correspondence: max.okraschevski@dlr.de

- (i) a consistent approximation of spatial derivatives by either a reproducing kernel (RK) or Moving-Least-Square (MLS) approach (Frontiere *et al.* 2017; Hopkins 2015).
- (ii) an Arbitrary-Lagrangian-Eulerian (ALE) formulation with transport velocity as noise mitigation technique, also rigorously incorporating particle shifting (Oger *et al.* 2016; Antuono *et al.* 2021b).

In line with these positive developments, the confidence into the ability of modern SPH methods to capture incompressible turbulence increases. Especially in complex multiphase flow situations these methods are nowadays optimistically combined with a Large Eddy Simulation (LES) perspective (Colagrossi *et al.* 2021; Lai *et al.* 2022; King *et al.* 2023; Meringolo *et al.* 2023). In the following, we will refer to this combination of modern SPH methods with LES simply as SPH-LES for brevity. As already mentioned by Bicknell (1991), such a confluence is intuitive since the SPH kernel and the LES low-pass filter, building the foundation of both methods, are mathematically congruent. Unfortunately, the development of rigorous combined SPH-LES theories is a very recent topic and scarcely addressed, e.g. Di Mascio *et al.* (2017); Antuono *et al.* (2021a); Okraschevski *et al.* (2022).

One central remaining issue is that all these modern SPH-LES studies intuitively model one of the central LES objects, namely the subfilter stress tensor τ_{SFS} , by classical, functional eddy viscosity approaches, employing the Boussinesq hypothesis (Schmitt 2007). In Okraschevski *et al.* (2022) we could argue for classical SPH, physically reinterpreting this method from a spatial coarse-graining perspective, that eddy viscosity modelling must fail due to the non-locality of the SPH method (Du & Tian 2020; Vignjevic *et al.* 2021; Yao *et al.* 2022). Yet, one might oppose that this is just a consequence of the classical SPH approach considered in our former study. This is where the following work comes into play showing that our coarse-graining perspective also generally applies to modern SPH methods. Hence, classical eddy viscosity modelling is compromising the most accurate prediction of turbulence possible and necessitates the development of completely new and specific subfilter stress models in the SPH-LES context. Implicit evidence pointing towards such a conclusion was also presented by Rennehan (2021).

2. Novelty and implications

In our former works (Okaschevski *et al.* 2021a,b) we laid the theoretical foundations to be summarized in Sec. 3 with Hardy’s theory (Hardy 1982) at its core. Based on it, we could demonstrate that SPH-LES with classical SPH seems fundamentally incompatible with explicit viscosity models due to the non-local characteristic of the discretization (Okaschevski *et al.* 2022). These works resulted in a PhD thesis (Okaschevski 2024). Here, we report evidence for the first time that this incompatibility also holds for SPH-LES with modern SPH methods, which are not plagued by the classical SPH problems as described in Sec. 1. As a consequence, we believe that classical eddy viscosity models for the subfilter stress tensor τ_{SFS} are detrimental in SPH-LES of incompressible turbulence and that novel models matching the discretization characteristics must be developed.

3. Coarse-graining perspective on modern SPH methods

Although modern SPH methods might not suffer from the same convergence issue as their original ancestor, at their heart they still employ quasi-Lagrangian \dagger particles. These are

\dagger This term is usually used within ALE frameworks (Vogelsberger *et al.* 2012; Oger *et al.* 2016; Antuono *et al.* 2021a). Here, we also include pseudo-Lagrangian (Vogelsberger *et al.* 2012) particles, also called purely Lagrangian particles in other works (Oger *et al.* 2016; Antuono *et al.* 2021a), into the definition.

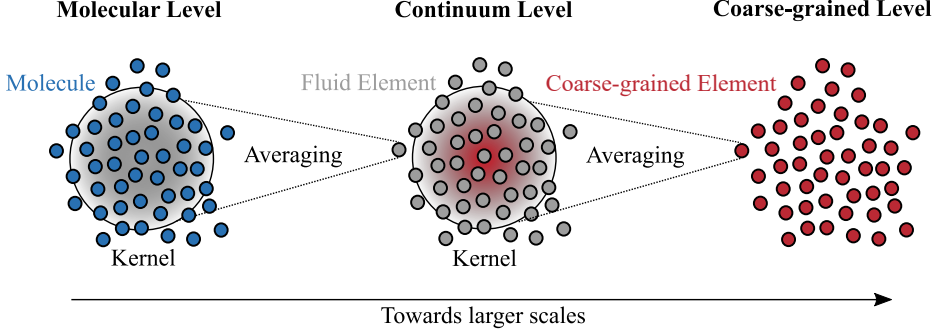


Figure 1: Illustration of spatial coarse-graining emerging from the generalization of Hardy's theory (Hardy 1982; Okraschevski *et al.* 2021b). Adapted from Okraschevski *et al.* (2022).

connected by a spherical, positive, and monotonously decaying kernel $W : \mathbb{R}^3 \rightarrow \mathbb{R}$ with compact support $V_{\mathbf{x}}$, being centered at the quasi-Lagrangian particles in $\mathbf{x} \in \mathbb{R}^3$. Hence, even modern SPH methods intrinsically contain two resolution scales, namely the mean particle distance Δl and the larger kernel diameter D_K . We termed this property *particle duality* in our former work (Okaschevski *et al.* 2022). This is a characteristic peculiarity compared to grid-based discretization techniques and results in strongly overlapping discretization elements, i.e. a non-local discretization. Despite the fact that numerical convergence in modern SPH methods can be reached using a constant ratio of $D_K/\Delta l = O(1)$ (Vila 1999; Hopkins 2015) resulting in a fixed number of neighbors N_{ngb} inside the kernel, one still might wonder which flow scales can be effectively resolved. Taking a conservative point of view, it must be expected that flow scales can be captured maximally up to the kernel diameter D_K . By means of such a rational, one implicitly interprets modern SPH methods from a spatial coarse-graining perspective at the effective scale D_K . Such a coarse-graining perspective is not only a convenient footing in the following, but also the physical foundation of the LES community (Eyink & Drivas 2018) and even more so a general perspective employed by fluid dynamicists (Irving & Kirkwood 1950; Okraschevski *et al.* 2021b; Eyink 2024). In the LES community the coarse-graining is also synonymously called *the filtering approach* (Germano 1992). Although the different terminologies describe equivalent mathematical operations, we believe that the term coarse-graining raises the awareness for a geometric interpretation in terms of a hierarchical clustering of Lagrangian particles (figure 1). The aforementioned can be vividly unravelled by generalizing the theory of Hardy from statistical physics (Hardy 1982; Okraschevski *et al.* 2021b) and highlights the conceptual similarity to the Lagrangian discretization techniques of interest. Hence, we anticipate that modern SPH methods aim at solving an effective field equation and intrinsically operate as Lagrangian Large Eddy Simulations. By defining the Lagrangian derivative as

$$\frac{d}{dt} := \partial_t + \tilde{\mathbf{v}} \cdot \nabla_{\mathbf{x}} \quad (3.1)$$

and the spatial coarse-graining of a scalar field $f : \mathbb{R}^3 \times \mathbb{R}_0^+ \rightarrow \mathbb{R}$ over $V_{\mathbf{x}}$ as

$$\bar{f}(\mathbf{x}, t) = \int_{V_{\mathbf{x}}} f(\mathbf{y}, t) W(\mathbf{x} - \mathbf{y}) d\mathbf{y} , \quad (3.2)$$

we will subsequently consider barotropic flows in a Lagrangian reference frame

$$\frac{d\bar{\rho}}{dt}(\mathbf{x}, t) = -\bar{\rho}(\mathbf{x}, t) \nabla_{\mathbf{x}} \cdot \tilde{\mathbf{v}}(\mathbf{x}, t) \quad (3.3)$$

$$\bar{\rho}(\mathbf{x}, t) \frac{d\tilde{\mathbf{v}}}{dt}(\mathbf{x}, t) = -\nabla_{\mathbf{x}} \bar{p}(\mathbf{x}, t) + \text{div}_{\mathbf{x}} [\tilde{\tau}_{visc} + \tau_{SFS}] (\mathbf{x}, t) \quad (3.4)$$

$$\bar{p}(\mathbf{x}, t) = \bar{p}_{ref} + c_s^2 (\bar{\rho}(\mathbf{x}, t) - \bar{\rho}_{ref}). \quad (3.5)$$

Moreover, we will assume for Eqs. (3.3), (3.4), (3.5) a weakly-compressible, low Mach number flow ($Ma < 0.3$). Hence, bulk viscous stresses are neglected. The fields $\bar{\rho}$ and \bar{p} denote the coarse-grained density and pressure, whereas $\tilde{\mathbf{v}} = \bar{\rho} \mathbf{v} / \bar{\rho}$ is the density-weighted coarse-grained velocity as proposed by Reynolds (1895), nowadays called Favre averaged velocity (Bilger 1975). For a Newtonian fluid, then, the viscous stress tensor reads

$$\tilde{\tau}_{visc} = \eta (\mathbf{J}_{\tilde{\mathbf{v}}} + \mathbf{J}_{\tilde{\mathbf{v}}}^T - \frac{2}{3} \nabla_{\mathbf{x}} \cdot \tilde{\mathbf{v}}) \quad (3.6)$$

with $\mathbf{J}_{\tilde{\mathbf{v}}}$ as Jacobian of $\tilde{\mathbf{v}}$. The dynamic viscosity η , the reference density $\bar{\rho}_{ref}$ and pressure \bar{p}_{ref} , as well as the speed of sound c_s are dealt as constant parameters to be specified.

The most important object emerging from the spatial coarse-graining at the arbitrary scale D_K is the subfilter stress tensor τ_{SFS} . It can be formally defined as (Vreman *et al.* 1994; Okraschevski *et al.* 2021b)

$$\tau_{SFS}(\mathbf{x}, t) := - \int_{V_x} \rho(\mathbf{y}, t) \mathbf{w}(\mathbf{x}, \mathbf{y}, t) \mathbf{w}^T(\mathbf{x}, \mathbf{y}, t) W(\mathbf{x} - \mathbf{y}) d\mathbf{y} = -\overline{\rho \mathbf{w} \mathbf{w}^T}(\mathbf{x}, t) \quad (3.7)$$

with \mathbf{w} denoting the peculiar velocity and \mathbf{w}^T its transpose. The peculiar velocity is a relative velocity connecting coarse-grained velocities $\tilde{\mathbf{v}}(\mathbf{x}, t)$ with associated continuum fluid element velocities $\mathbf{v}(\mathbf{y}, t)$ (figure 1). As convention, we label and distinguish the spatial coordinates of fluid elements by $\mathbf{y} \in \mathbb{R}^3$ and of coarse-grained elements by the spatial coordinate $\mathbf{x} \in \mathbb{R}^3$. Consequently, the peculiar velocity is a non-local quantity by definition and emerges from

$$\mathbf{w}(\mathbf{x}, \mathbf{y}, t) = \mathbf{v}(\mathbf{y}, t) - \tilde{\mathbf{v}}(\mathbf{x}, t). \quad (3.8)$$

The velocity decomposition is illustrated in figure 2. We argue that \mathbf{w} is the physically appropriate fluctuating velocity field in the coarse-graining framework. It satisfies $\overline{\rho \mathbf{w}} = 0$ by construction (Okaschevski *et al.* 2021b) and does not require the introduction of generalized central moments to identify the averaging invariance of the turbulent equations (Germano 1992). Since the velocities $\mathbf{v}(\mathbf{y}, t)$ of the fluid elements are unknown at the coarse-grained level, we practically face the well-known closure problem for the SFS tensor τ_{SFS} in equation (3.7).

For turbulent flows at finite resolution, the closure problem is usually resolved by explicit modelling of τ_{SFS} with functional eddy viscosity approaches (Silvis *et al.* 2017; Moser *et al.* 2021). However, it can be also verified by means of statistical physics that classical and modern SPH methods contain significant implicit SFS due to their kernel-based discretization with quasi-Lagrangian particles. (Posch *et al.* 1995; Ellero *et al.* 2010; Borreguero *et al.* 2019; Okraschevski *et al.* 2021a). Considering both of these contributions, it is natural to ask how the explicit and implicit SFS contributions interact and if implicit SFS contributions can be reduced by explicit models of τ_{SFS} ? This is the leading theme of this work and in the spirit of similar works in the grid-based LES community, e.g. Ghosal (1996); Dairay *et al.* (2017).

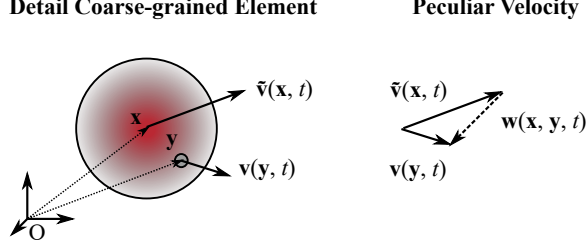


Figure 2: Visualization of the velocity decomposition in Equation (3.8).
Adapted from Okrashevski (2024).

4. Methods

There is a large variety of modern SPH methods today as contrasted by Eirís *et al.* (2023). Hence, care must be taken in the choice of the modern SPH method for the verification of our incompatability-hypothesis concerning SPH-LES with eddy viscosity models. We decided to use the locally conservative and second-order accurate meshless finite-mass method (MFM), developed and made publicly available in the open source code GIZMO by Hopkins (2015). Since MFM belongs to the large class of modern SPH methods termed as MLS-SPH-ALE (Eirís *et al.* 2023), it inherently incorporates both strategies mentioned in Sec. 1 to eliminate the convergence issues of classical SPH. MFM is based on a ALE formulation without particle shifting, which can be operated either in fully Eulerian or quasi-Lagrangian mode, although we will only use the latter. We are convinced that the Lagrangian character is still a key argument for the discretization of fluid flows with modern SPH methods, giving natural access to Lagrangian flow properties like Lagrangian Coherent Structures (Haller 2015; Dauch *et al.* 2018). Applying the MFM method to Eqs. (3.3), (3.4), (3.5) with a second-order accurate MLS approximation of spatial derivatives, one arrives, $\forall i \in \{1, \dots, N\}$ particles with mass M_i , at

$$\frac{dM_i}{dt} = 0 \implies \bar{\rho}_i = M_i \sum_{j=1}^{N_{ngb}} W(\mathbf{x}_i - \mathbf{x}_j) \quad (4.1)$$

$$M_i \frac{d\mathbf{v}_i}{dt} = \sum_{j=1}^{N_{ngb}} -\bar{p}_{ij}^* \mathbf{A}_{ij}^{eff} + \left[\tilde{\tau}_{visc,ij}^* + \tau_{SFS,ij}^* \right] \mathbf{A}_{ij}^{eff} \quad (4.2)$$

$$\bar{p}_i = \bar{p}_{ref} + c_s^2 (\bar{\rho}_i - \bar{\rho}_{ref}), \quad (4.3)$$

where we use standard particle notation. Thus, the single index i indicates the numerical proxy of the corresponding field at \mathbf{x}_i . The discretized momentum equation (4.2) can be interpreted as a Lagrangian finite volume formulation with fluxes to be approximated at effective interface areas $\mathbf{A}_{ij}^{eff} \in \mathbb{R}^3$ between particles i and j . These interface areas depend on the local particle configuration and the chosen kernel, subsequently the pairing-stable Wendland C4 with $N_{ngb} = 128$ as our default (Dehnen & Aly 2012). The interface fluxes, namely $\bar{p}_{ij}^* \in \mathbb{R}$ and $\tilde{\tau}_{visc,ij}^*, \tau_{SFS,ij}^* \in \mathbb{R}^{3 \times 3}$, are computed with approximate Riemann solvers that are slope- and flux-limited. More details on the computation of the effective interface areas \mathbf{A}_{ij}^{eff} , the Harten-Lax-van Leer contact (HLLC) solver for \bar{p}_{ij}^* , the Harten-Lax-van Leer (HLL) solver for $\tilde{\tau}_{visc,ij}^*, \tau_{SFS,ij}^*$ and aspects beyond that can be found in the works of Hopkins (2015, 2016). We want to note that the resulting system of Eqs. (4.1), (4.2),

(4.3) is very similar to the well-known classical weakly-compressible SPH (WCSPH). Thus, we will term it accordingly as weakly-compressible MFM (WCMFM). The discretization is obviously non-local realizing that the differential operators in the momentum balance of equation (3.4) are transferred to N_{ngb} flux evaluations per particle on the kernel scale D_K , which is in the spirit of classical SPH (Du & Tian 2020; Vignjevic *et al.* 2021; Yao *et al.* 2022). As will be demonstrated in Sec. 5, it seems to be exactly this non-locality in combination with the quasi-Lagrangian particles that leads to the incompatibility of SPH-LES with eddy viscosity models for incompressible turbulence.

As a canonical benchmark we will consider a Taylor-Green flow (Taylor & Green 1937) on the periodic domain $\Omega = [0, 2\pi]^3$ for three different particle counts of $N \in [128^3, 256^3, 512^3]$. This is a precious test to evaluate the dissipation characteristics of a numerical solver and its ability to resolve incompressible turbulence, e.g. (Brachet *et al.* 1983; Drikakis *et al.* 2007; Moura *et al.* 2017; Dairay *et al.* 2017; Pereira *et al.* 2021; Fehn *et al.* 2022). As in our former work with classical SPH (Okraschevski *et al.* 2022), we will use the DNS solution of Dairay *et al.* (2017) at $Re = 10^4$ as a reference. It was computed with the sixth-order finite difference code Incompact3d (Laizet & Li 2011). We will initialize and evaluate the WCMFM simulations exactly as we did in Okraschevski *et al.* (2022) for classical WCSPH. Thus, we will specify the initial rms Mach number as $Ma_{rms}(t = 0 \text{ s}) = \sqrt{2e_v(t = 0 \text{ s})}/c_s = 0.1$ such that $c_s = 5 \text{ m/s}$, $\bar{\rho}_{ref} = 1 \text{ kg/m}^3$ and $\bar{p}_{ref} = \bar{\rho}_{ref}c_s^2/4 = 6.25 \text{ Pa}$ in equation (4.3). Consequently, the dynamic viscosity in equation (3.6) must be $\eta = 0.0001 \text{ Pas}$ to reach the targeted Reynolds number. We will study and compare the temporal evolution of the averaged kinetic energy e_v , its corresponding averaged dissipation rate $\epsilon_t = -\frac{de_v}{dt}$ and the spectral energy density $E(k)$ at $t = 14 \text{ s}$. The time instance was selected in accordance with Dairay *et al.* (2017), which ensures that the turbulence is developed and exhibits the expected inertial range scaling of $E(k) \sim k^{-5/3}$ (Kolmogorov 1941; Obukhov 1941; Onsager 1945; Heisenberg 1948) [†]. For the evaluation of the spectra, we use the validated methodology of Bauer & Springel (2012) in combination with considerations by Durran *et al.* (2017). This preserves physically important small-scale features of the flow and guarantees the validity of the discrete Parseval relation.

Finally, to work out the interplay between explicit and implicit SFS, we need to specify an explicit SFS model and think about how the implicit SFS contribution can be estimated. For the former, we decided to opt for the σ -model by Nicoud *et al.* (2011), which is one of the most sophisticated static eddy viscosity models. It eliminates artificial dissipation in two-dimensional flows, laminar shear zones and in case of solid body rotation but likewise shows proper asymptotic scaling near walls (Nicoud *et al.* 2011; Silvis *et al.* 2017; Moser *et al.* 2021). The explicit model reads in continuous representation

$$\tau_{SFS}^{exp} = \eta_{SFS}(\mathbf{J}_{\tilde{\mathbf{v}}} + \mathbf{J}_{\tilde{\mathbf{v}}}^T - \frac{2}{3}\nabla_{\mathbf{x}} \cdot \tilde{\mathbf{v}}), \quad \eta_{SFS} := \bar{\rho}(C_{\sigma}\Delta)^2 \frac{(\sigma_1 - \sigma_2)(\sigma_2 - \sigma_3)\sigma_3}{\sigma_1^2}, \quad (4.4)$$

with $\sigma_k, k \in \{1, 2, 3\}$, being the singular values of the tensor $\mathbf{J}_{\tilde{\mathbf{v}}}^T \mathbf{J}_{\tilde{\mathbf{v}}}$, $C_{\sigma} = 1.35$ as model constant and the filter width $\Delta = D_K$. The latter is an unambiguous choice emerging from our coarse-graining perspective and a matter of debate in the SPH-LES context (Rennehan 2021; King *et al.* 2023). We will elaborate on it more closely in Sec. 5. For the estimation of the implicit SFS tensor we assume that density changes of the fluid elements over the kernel scale D_K are much weaker than the corresponding velocity changes. This is reasonable for a weakly-compressible flow developing characteristics of incompressible turbulence and

[†] Note that there is recent experimental doubt on the quantitative correctness of this scaling in the inertial range (Küchler *et al.* 2023).

implies that $\tilde{\mathbf{v}} = \bar{\mathbf{v}}$. Then, with the spatial coarse-graining operation in equation (3.2) and linearization of the continuum velocity field at a position $\mathbf{z} \in \mathbb{R}^3$, one obtains $\tilde{\mathbf{v}}(\mathbf{x} = \mathbf{z}, t) = \mathbf{v}(\mathbf{y} = \mathbf{z}, t) + O(D_K^2)$, which gives a consistency preserving (with respect to the MFM discretization) second-order proxy for the peculiar velocity in equation (3.8), namely

$$\mathbf{w}(\mathbf{x}_1, \mathbf{x}_2, t) \approx \tilde{\mathbf{v}}(\mathbf{x}_2, t) - \tilde{\mathbf{v}}(\mathbf{x}_1, t) \quad (4.5)$$

with two different coarse-grained coordinates $\mathbf{x}_1, \mathbf{x}_2$. Inserting equation (4.5) into the SFS tensor in equation (3.7) gives, after discretization of the integral into finite-mass elements, the following estimator for the implicit SFS in particle notation

$$\tau_{SFS,i}^{imp} \approx - \sum_{j=1}^{N_{ngb}} (\tilde{\mathbf{v}}_j - \tilde{\mathbf{v}}_i)(\tilde{\mathbf{v}}_j - \tilde{\mathbf{v}}_i)^T W(\mathbf{x}_i - \mathbf{x}_j) M_j. \quad (4.6)$$

Since incompressible turbulence is a convection driven phenomenon, we will evaluate the local importance of the implicit SFS on a particle i in comparison to the coarse-grained convective stress tensor $\bar{\rho}_i \tilde{\mathbf{v}}_i \tilde{\mathbf{v}}_i^T$. Therefore, we define the R-index as

$$R_i := \frac{\|\tau_{SFS,i}^{imp}\|_F}{\|\tau_{SFS,i}^{imp}\|_F + \|\bar{\rho}_i \tilde{\mathbf{v}}_i \tilde{\mathbf{v}}_i^T\|_F} \quad (4.7)$$

with $\|\cdot\|_F$ denoting the Frobenius norm.

5. Results & Discussion

In this section, we will present and critically discuss the results of our study. We start with a qualitative verification of our implementation of the σ -model (Nicoud *et al.* 2011) in equation (4.4) into the code GIZMO (Hopkins 2015). Therefore, the uniquely colored individual particle IDs are utilized as flow tracers and visualized for the purpose of structure identification (figure 3). Two snapshots before and after the well-known dissipation peak (Brachet *et al.* 1983), namely at $t_{1,2} = 9 \pm 3$ s, are shown in the first and second column of figure 3 for the highest resolution runs $N = 512^3$. They vividly render the development of primary instabilities and turbulence in the flow field. The first row displays the case without explicit SFS model (WCMFM), the second with explicit SFS model (WCMFM + SIGMA). In the third row, the central quantity of the σ -model, namely the eddy viscosity field according to equation (4.4), is shown. It is scaled by the dynamic viscosity of the flow. The ratio is denoted as η^* , visually correlates with the flow structures and is evidently non-negligible in the shear flow planes (figure 3a) where incompressible turbulence develops. In this region the eddy viscosity is dominant over the dynamic viscosity by up to an order of magnitude. This is an anticipated consequence as the coarse-grained viscous stress tensor is bounded from above by the Cauchy-Schwarz inequality and it can be proven that the bound scales with $1/D_K$ (Eyink & Drivas 2018). Hence, for regions of underresolved turbulence, in which the kernel scale D_K is larger than viscous length scale, one would expect $\eta^* \gg 1$. A comparison of the flow structures predicted by WCMFM and WCMFM + SIGMA reveals that the explicit SFS model does not inhibit the dynamics of the primary instabilities before the dissipation peak (figure 3a vs. 3c). However, it apparently damps noisy small-scale features in the turbulent flow field after the dissipation peak (figure 3b vs. 3d). This could be incorrectly interpreted as removal of numerically dissipative noise related to an artificial thermalization. As extensively discussed by Dairay *et al.* (2017) for grid-based methods, the removal of such an artificial thermalization should be the ultimate goal of an explicit SFS model, eventually resulting in a quantitative improvement for the dissipation characteristics in physical and spectral space.

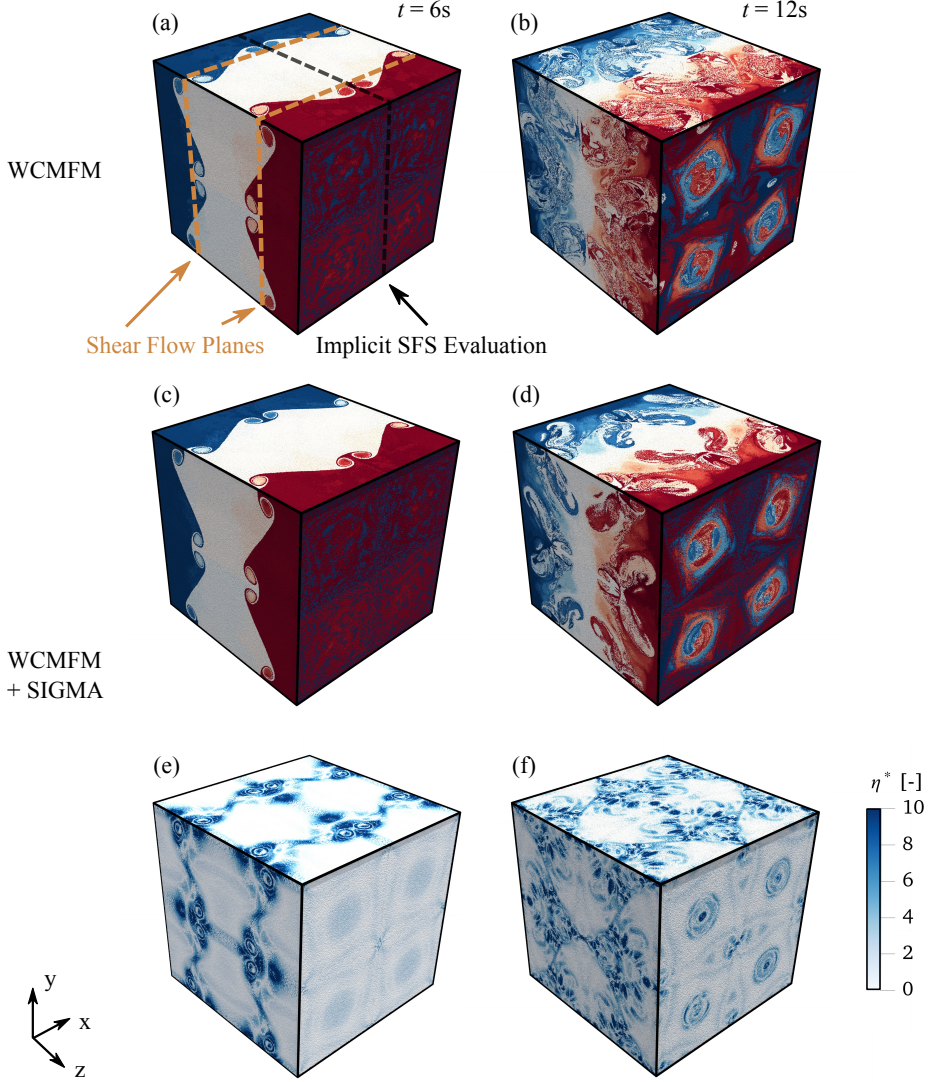


Figure 3: Qualitative verification of the implementation of the σ -model (Nicoud *et al.* 2011) for $N = 512^3$. (a,b) Flow structures before and after the dissipation peak for the case without explicit SFS model (WCMFM) and (c,d) for the case with explicit SFS model (WCMFM + SIGMA). In (e,f) the scaled eddy viscosity field is displayed.

We will show now that the explicit SFS model completely fails with respect to such a quantitative analysis although visually it seems to perform well.

Therefore, we compare the temporal evolution of the averaged kinetic energy e_v , the averaged dissipation rate ϵ_t and the spectral energy density $E(k, t = 14s)$ in figure 4. The latter is scaled with the corresponding kinetic energy value $e_v(t = 14s)$ and $L_c = 1$ m, such that integration over the wavenumber shells always results in unity. Cases without explicit SFS model (WCMFM) are displayed as solid blue lines, whereas cases with explicit SFS model (WCMFM + SIGMA) are displayed as red dashed lines. It is evident for the kinetic energy evolution in figure 4a that qualitative convergence towards the DNS (solid black line) for increasing particle count can be obtained. After the dissipation peak, as soon as

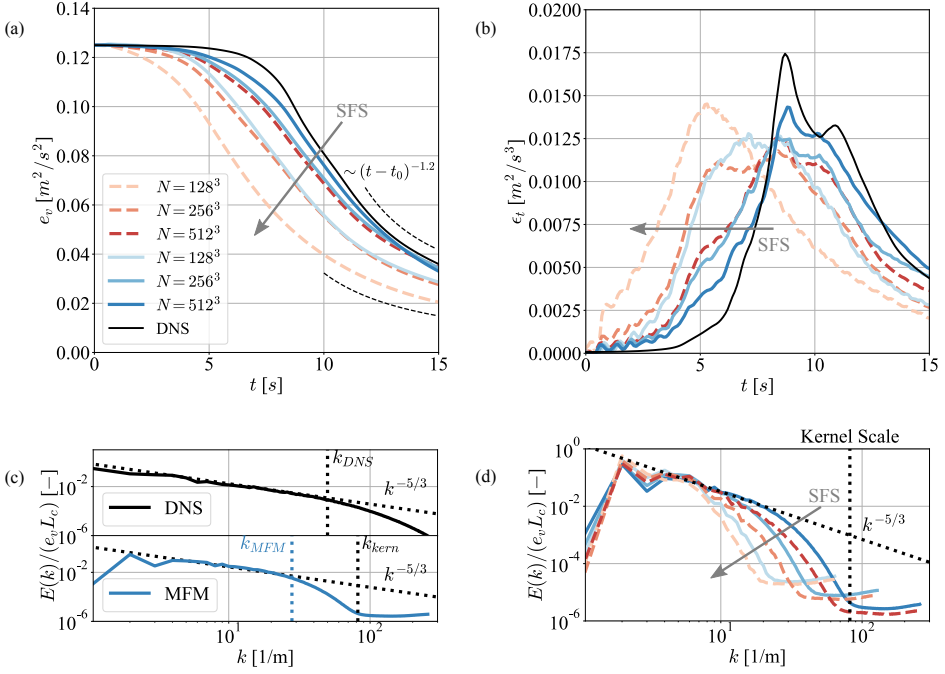


Figure 4: Quantitative effect of the σ -model (Nicoud *et al.* 2011) in physical and spectral space for different resolutions. (a) Averaged kinetic energy, (b) Averaged dissipation rate, (c) Scaled spectral energy density at $t = 14$ s for DNS and WCMFM run ($N = 512^3$) without explicit SFS model. (d) Scaled spectral energy density at $t = 14$ s. For orientation the kernel scale for $N = 512^3$ is included.

incompressible turbulence develops, the theoretically predicted Saffman decay rate (Skrbek & Stalp 2000) of $e_v \sim (t - t_0)^{-1.2}$ can be matched (dashed black line). Here, t_0 denotes a time shift parameter which accounts for the earlier transitions at lower resolution. These observations are independent of the explicit SFS model and also reflected by the dissipation rate profiles in figure 4b. However, the results clearly demonstrate the detrimental effect of the eddy viscosity model on the dissipation characteristics in physical space. Coincidentally, for the chosen configuration, it seems that the explicit SFS model leads to a fallback of the accuracy by roughly a whole resolution step. The WCMFM cases for $N = 128^3$ and $N = 256^3$ behave very similar to the WCMFM + SIGMA cases for $N = 256^3$ and $N = 512^3$. In other words, under ideal code scaling with CFL restriction, to achieve the same result with an explicit SFS model at least an $2^4 = 16$ times higher computational effort is required. This is a quite drastic finding. Note that for a quasi-Lagrangian particle method the highest resolution WCMFM run ($N = 512^3$) without explicit SFS model leads to a comparably accurate prediction of the dissipation characteristics in physical space. Especially, the sharper prediction of the global dissipation peak and the local peak nearby in figure 4b compared to WCMFM with twice as many neighbors (Okaschevski *et al.* 2022) is prominent.

Before we proceed with the comparison on the spectral dissipation characteristics for all resolutions, we will first elaborate on the highest resolution WCMFM run in figure 4c. Provably, WCMFM as modern SPH method is able to predict the inertial range scaling of incompressible turbulence by about an order of magnitude in wave number space. However,

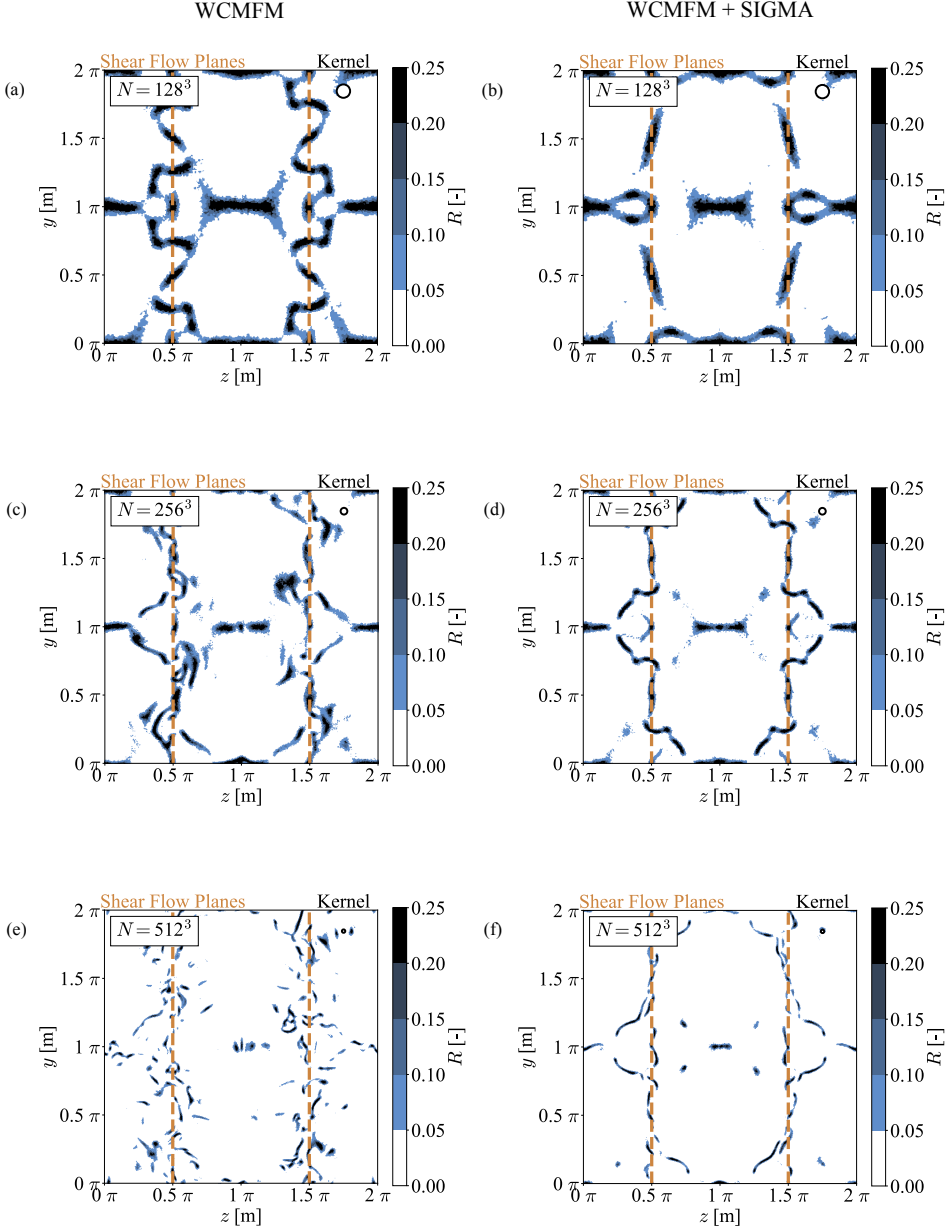


Figure 5: Implicit SFS measured by the R-index in equation 4.7 at the plane $x = \pi$ for the time $t = 14$ s. Different resolutions are shown without explicit SFS model (WCMFM) and with explicit SFS model (WCMFM + SIGMA).

in comparison to the DNS case the inertial range already terminates at $k_{MFM} < k_{DNS}^\dagger$, then passes into an energy deficit range $k \in [k_{MFM}; k_{kern}]$ and is followed by an artificial thermalization resulting from kernel scale errors. Qualitatively, this is similar to classical

[†] By k_{MFM} we denote the effective wavenumber up to which a qualitatively correct spectral behavior can be observed and not the wavenumber corresponding to the mean particle diameter Δl .

SPH and happens although the kernel wavelength satisfies $k_{\text{kernel}} > k_{\text{DNS}}$ (Okraschevski *et al.* 2022). It is indicative for the non-local character of the method, the emerging implicit SFS according to equation 4.6 and a reaction to peculiar velocities on the kernel scale, which manifest as artificial thermalization. In the next paragraph this will be detailed, but prior to that we want to show in figure 4d that the explicit SFS model also deteriorates the situation in spectral space due to the non-locality of the method. Instead of removing a significant part of kinetic energy from the artificial thermalization, it dominantly withdraws kinetic energy from the energy deficit range and the partially resolved inertial range. Hence, it erroneously attacks scales which are already badly resolved and not the numerically dissipative ones. While these observations should be sufficient to advise against the usage of classical eddy viscosity models in the SPH-LES context, we want to unravel the interplay of the implicit SFS and the explicit SFS model in the following paragraph and underpin these spectral observations in physical space.

Ergo, we will visualize the implicit SFS relative to the convective stress using the R-index defined in equation 4.7 and investigate how the field is affected by resolution and the explicit SFS model. We will focus on the plane $x = \pi$ (figure 3a) for the time $t = 14$ s, exactly corresponding to the spectra in figure 4c and 4d. The resulting fields are depicted in figure 5 and contain a kernel element at the given resolution in the upper right corner to assess the extent of emerging coherent structures. We will start with influence of the spatial resolution for WCMFM without explicit SFS model shown in the first column. Note that due to the definition of the R-index the exact ratio of implicit SFS to the convective stress is given by $||\tau_{\text{SFS},i}^{\text{imp}}||_F / ||\bar{\rho}_i \tilde{\mathbf{v}}_i \tilde{\mathbf{v}}_i^T||_F = R_i / (1 - R_i)$ and the upper limit of the colorbar indicates that the implicit SFS is a third of the convective stress. Interestingly, for all resolutions, the implicit SFS is only relevant around the shear flow planes where incompressible turbulence develops and forms a coherent network that surpasses the kernel scale. Although, the coherent network becomes more delicate for higher resolution (cp. figure 5a and 5e), structures with significant contribution remain larger in extent than the given kernel element. Considering that the implicit SFS is a consequence of the peculiar velocities evaluated at the kernel scale but unfolds its effect well beyond the kernel scale, we believe to see the deterministic reason for how the artificial thermalization causes the energy deficit range in spectral space (figure 4c and 4d). Hence, the $||\tau_{\text{SFS},i}^{\text{imp}}||_F$ field unravels how kernel scale effects propagate to larger scales due to the non-local character of the method. Focusing now on the second column, in which the WCMFM + SIGMA cases are shown, a reflection of the spectral behavior in figure 4d can be clearly seen as well. Even though we would expect for a working explicit SFS model to significantly reduce $||\tau_{\text{SFS},i}^{\text{imp}}||_F$ resp. R on the kernel scale, we see a strong non-local damping. The network itself is destroyed, instead of diminishing its amplitude. Recalling the similarity of the WCMFM cases for $N = 128^3$ and $N = 256^3$ and WCMFM + SIGMA cases for $N = 256^3$ and $N = 512^3$ in physical space highlighted above, our requirements on a working explicit SFS model can be specified more precisely. It manifests in the comparison of figure 5a vs. 5d and figure 5c vs. 5f. There, the network structure is mainly preserved and the amplitude of R diminished. Together with the spectral statistics in figure 4d, it is evident that this observation correlates with a diminished artificial thermalization and gain in the energy deficit range. This is what we would expect from an explicit SFS model in the SPH-LES context in a much stronger form for a *fixed* resolution but unfortunately see that even sophisticated eddy viscosity models, like the σ -model by Nicoud *et al.* (2011), fail.

Taking this new evidence for a modern SPH method into account with our former, congruent results for classical SPH (Okraschevski *et al.* 2022), we are convinced that SPH-LES with classical eddy viscosity models is highly detrimental for the prediction of incompressible turbulence. In our opinion this is due to the mismatch of discretization

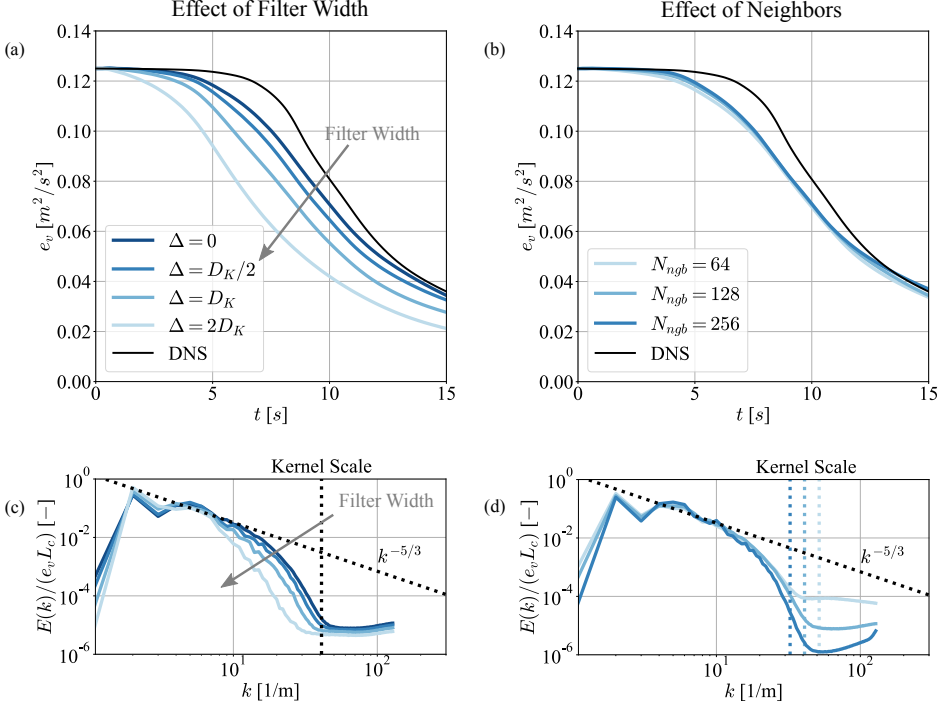


Figure 6: (a,c) Influence of the filter width Δ for WCMFM + SIGMA and (b,d) the neighbor particles N_{ngb} for WCMFM without explicit SFS model. All simulations were performed with $N = 256^3$.

characteristics, namely quasi-Lagrangian particles and non-locality, with the explicit SFS model assumptions being solely physics motivated. We observe the well-known issue from grid-based LES that an *a priori* correct model can perform badly in simulations *a posteriori* (Park *et al.* 2004; Dairay *et al.* 2017). From our coarse-graining perspective modern SPH methods operate intrinsically as Lagrangian Large Eddy Simulations with implicit SFS for incompressible turbulence. We want to stress that the chosen terminology is not indicative on the quality of this implicit LES approach, which manifests in the spectral energy density in figure 4c. Obviously, it is plagued by an energy deficit range due to artificial thermalization. We have shown already in our former work that the inertial range can be reproduced with a grid-based finite volume Smagorinsky LES at much lower resolution of $N = 384^3$ and lower computational cost (Okraschewski *et al.* 2022).

Before we finally conclude our work, we want to address two further aspects which are not less important. Namely, the effect of the filter width Δ when using an explicit SFS model and the effect of the neighbor particles N_{ngb} for simulations without explicit SFS model. The results for $N = 256^3$ are displayed in figure 6. The first aspect is an ongoing matter of debate in the SPH-LES context (Rennehan 2021; King *et al.* 2023). Although from our coarse-graining perspective the choice $\Delta = D_K$ is unambiguous, we have considered the two further cases with $\Delta = D_K/2$ (Rennehan 2021) and $\Delta = 2D_K$. The case $\Delta = 0$ corresponds to the run without an explicit SFS model. Obviously from figure 6a and figure 6c, we observe a monotonous trend with increasing filter width. The effect is detrimental in physical space as well as in spectral space, but starts to get irrelevant for $\Delta \leq D_K/2$. This is congruent with the observation of Rennehan (2021), who studied forced subsonic turbulence with MFM

and different explicit SFS models using a dynamic procedure. It prompts the eventuality that SPH-LES studies with Δ equal or smaller than the kernel radius, e.g. Antuono *et al.* (2021b); Colagrossi *et al.* (2021); Lai *et al.* (2022); King *et al.* (2023), just run (slightly) more expensive simulations in which the influence of the explicit SFS model is negligible. The second aspect concerns the influence of the number of neighbors N_{ngb} for WCMFM without explicit SFS model. In classical SPH better convergence towards the DNS can be obtained by increasing N_{ngb} (Zhu *et al.* 2015; Okraschevski *et al.* 2022), which is in the spirit of explicitly filtered LES (Lund 2003; Bose *et al.* 2010). However, for modern SPH methods as MFM one would expect minor influence of N_{ngb} by construction (Vila 1999; Hopkins 2015). Indeed, a negligible influence is found according to 6b and figure 6d for the well-resolved scales. Merely in spectral space we see a loss of kinetic energy from the artificial thermalization and the energy deficit range which seems irrelevant for the physical space dynamics. This is contrary to classical SPH, practically eliminates N_{ngb} as crucial calibration parameter and is beneficial for the computational cost at finite resolution. Coincidentally, we observe for $N_{ngb} \neq 128$ that the associated kernel scale in figure 6d is not perfectly separating the energy deficit range and the artificial thermalization as in the former cases.

6. Concluding Remarks

In this study, we presented evidence for the incompatibility of modern SPH methods and classical eddy viscosity models for scale-resolved incompressible turbulence. With our coarse-graining perspective, we could argue and show for MFM, as a representative from the class of MLS-SPH-ALE approaches (Eirís *et al.* 2023), that it intrinsically operates as Lagrangian Large Eddy Simulation with significant implicit SFS. Even a sophisticated eddy viscosity model like the σ -model by Nicoud *et al.* (2011) is not able to reduce this implicit SFS due to the non-locality of the discretization method. For the unambiguous filter width $\Delta = D_k$ the explicit SFS model attacks dominantly scales larger than the kernel which are already underresolved. Hence, the explicit SFS model is either highly detrimental physically or, for choices of $\Delta \leq D_K/2$, likely irrelevant and introduces computational overhead. The latter complies with results of Rennehan (2021). To our knowledge such a study of the interplay between implicit SFS and explicit SFS model for a modern SPH method is presented for the first time, revealing the familiar *a priori* vs. *a posteriori* dilemma in grid-based LES, e.g. (Park *et al.* 2004; Dairay *et al.* 2017).

We want to stress that our coarse-graining theory is only valid for $D_K \approx \text{const.}$ and $\rho \approx \text{const.}$, hence, when compressibility effects are negligible. This is what we ensured by our initial rms Mach number choice $Ma_{rms}(t = 0 \text{ s}) = \sqrt{2e_v(t = 0 \text{ s})}/c_s = 0.1 < 0.3$ (Jakobsen 2014) for the decaying Taylor-Green flow at $Re = 10^4$. Considering this aspect, an essential difference between our results and the results of Rennehan (2021) should be highlighted. The energy deficit range observed in this study and our former one for classical SPH (Okraschevski *et al.* 2022), is there replaced by an energy pile-up known from highly accurate discontinuous Galerkin methods (Moura *et al.* 2017; Fehn *et al.* 2022). We believe this difference is rooted in the Mach number at which the spectral statistics are computed. Whereas $Ma_{rms} \approx 0.3$ is controlled by forcing in Rennehan (2021), the Mach number in our decaying case can be estimated to be $Ma_{rms}(t = 14 \text{ s}) = \sqrt{2e_v(t = 14 \text{ s})}/c_s \approx 0.06$. It was already shown by Hopkins (2015) that the accuracy of the MFM method deteriorates with lower Mach number, possibly explaining the switch from the energy pile-up to the energy deficit also known from classical SPH. Such low Mach numbers are not unusual in engineering applications and favorably comply with our coarse-graining theory.

Finally, we want to hypothesize how two mainstream aspects of modern SPH methods,

not considered in this study, might fit into our findings. Nowadays, particle shifting and density diffusion are established numerical noise mitigation techniques, also in the SPH-LES context (Antuono *et al.* 2021a,b; Colagrossi *et al.* 2021; Meringolo *et al.* 2023). It is likely that both reduce the peculiar velocities on the kernel scale according to equation 4.5 and indirectly have positive feedback on the implicit SFS according to equation 4.6. However, we believe that the density diffusion, that can be heuristically rationalized by a coarse-graining without the density-weighted Favre velocity (Di Mascio *et al.* 2017), will be also plagued by non-local effects of the discretization scheme. Very likely, it will not only mitigate noisy but also physically underresolved scales. Nevertheless, this needs to be tested in follow-up studies.

All in all we are convinced that SPH-LES approaches, even with modern SPH methods, must focus on the mitigation of the implicit SFS. Either directly by completely new explicit SFS models which match the discretization characteristics of modern SPH methods or indirectly by numerical noise mitigation techniques.

Acknowledgements. The authors acknowledge support by the state of Baden-Württemberg through bwHPC. Moreover, the authors would like to thank Shreyas Joshi for critical feedback on the manuscript as well as for valuable discussions.

Funding. This research received no specific grant from any funding agency, commercial or not-for-profit sectors.

Declaration of interests. The authors report no conflict of interest.

Author ORCIDs. M. Okraschevski, <https://orcid.org/0000-0001-8296-7327>; N. Bürkle, <https://orcid.org/0000-0002-9380-8716>; M. Wicker, <https://orcid.org/0009-0009-5255-6936>.

REFERENCES

- ANTUONO, M., MARRONE, S., MASCIIO, A. DI & COLAGROSSI, A. 2021a Smoothed particle hydrodynamics method from a large eddy simulation perspective. Generalization to a quasi-Lagrangian model. *Phys. Fluids* **33**, 015102.
- ANTUONO, M., SUN, P.N., MARRONE, S. & COLAGROSSI, A. 2021b The δ -ALE-SPH model: An arbitrary Lagrangian-Eulerian framework for the δ -SPH model with particle shifting technique. *Comput. Fluids* **216**, 104806.
- BAUER, A. & SPRINGEL, V. 2012 Subsonic turbulence in smoothed particle hydrodynamics and moving-mesh simulations. *Mon. Not. R. Astron. Soc.* **423**, 2558.
- BICKNELL, G. V. 1991 The Equations of Motion of Particles in Smoothed Particle Hydrodynamics. *SIAM J. Sci. Statist. Comput.* **12**, 1198–1206.
- BILGER, R. W. 1975 A note on favre averaging in variable density flows. *Combust. Sci. Technol.* **11**, 215–217.
- BORREGUERO, M., BEZGIN, D., ADAMI, S. & ADAMS, N. A. 2019 Implicit atomistic viscosities in smoothed dissipative particle dynamics. *Phys. Rev. E* **100**, 033318.
- BOSE, S. T., MOIN, P. & YOU, D. 2010 Grid-independent large-eddy simulation using explicit filtering. *Phys. Fluids* **22** (10), 105103.
- BRACHET, M., MEIRON, D., ORSZAG, S., NICKEL, B., MORF, R. & FRISCH, U. 1983 Small-scale structure of the taylor–green vortex. *J. Fluid Mech.* **130**, 411–452.
- COLAGROSSI, A., MARRONE, S., COLAGROSSI, P. & TOUZÉ, D. LE 2021 Da Vinci’s observation of turbulence: A French-Italian study aiming at numerically reproducing the physics behind one of his drawings, 500 years later. *Phys. Fluids* **33** (11), 115122.
- COLAGROSSI, A., SOUTO-IGLESIAS, A., ANTUONO, M. & MARRONE, S. 2013 Smoothed-particle-hydrodynamics modeling of dissipation mechanisms in gravity waves. *Phys. Rev. E* **87**, 023302.
- DAIRAY, T., LAMBALLAIS, E., LAIZET, S. & VASSILICOS, J. C. 2017 Numerical dissipation vs. subgrid-scale modelling for large eddy simulation. *J. Comput. Phys.* **337**, 252–274.
- DAUCH, T. F., RAPP, T., CHAUSSONNET, G., BRAUN, S., KELLER, M.C., KADEN, J., KOCH, R., DACHSBACHER, C. & BAUER, H.-J. 2018 Highly efficient computation of finite-time lyapunov exponents (ftle) on gpus based on three-dimensional sph datasets. *Computers & Fluids* **175**, 129–141.

- DEHNEN, W. & ALY, H. 2012 Improving convergence in smoothed particle hydrodynamics simulations without pairing instability. *Mon. Not. R. Astron. Soc.* **425**, 1068—1082.
- DI MASCIIO, A., ANTUONO, M., COLAGROSSI, A. & MARRONE, S. 2017 Smoothed particle hydrodynamics method from a large eddy simulation perspective. *Phys. Fluids* **29**, 035102.
- DRIKAKIS, D., FUREBY, C., GRINSTEIN, F. F. & YOUNGS, D. 2007 Simulation of transition and turbulence decay in the taylor–green vortex. *J. Turbul.* **8**, N20.
- DU, Q. & TIAN, X. 2020 Mathematics of Smoothed Particle Hydrodynamics: A Study via Nonlocal Stokes Equations. *Found. Comput. Math.* **20**, 801–826.
- DURRAN, D., WEYN, J. A. & MENCHACA, M. Q. 2017 Practical considerations for computing dimensional spectra from gridded data. *Mon. Weather Rev.* **145**, 3901—3910.
- EIRÍS, A., RAMÍREZ, L., COUCEIRO, I., FERNÁNDEZ-FIDALGO, J., PARÍS, J. & NOGUEIRA, X. 2023 MLS-SPH-ALE: A Review of Meshless-FV Methods and a Unifying Formulation for Particle Discretizations. *Arch. Computat. Methods. Eng.* **30**, 4959–4981.
- ELLERO, M., ESPAÑOL, P. & ADAMS, N.A. 2010 Implicit atomistic viscosities in smoothed particle hydrodynamics. *Phys. Rev. E* **82**, 046702.
- EYINK, G. 2024 Onsager’s ‘ideal turbulence’ theory. *J. Fluid Mech.* **988**, P1.
- EYINK, G. L. & DRIVAS, T. D. 2018 Cascades and Dissipative Anomalies in Compressible Fluid Turbulence. *Phys. Rev. X* **8**, 011022.
- FEHN, N., KRONBICHLER, M., MUNCH, P. & WALL, W. A. 2022 Numerical evidence of anomalous energy dissipation in incompressible euler flows: towards grid-converged results for the inviscid taylor–green problem. *J. Fluid Mech.* **932**, A40.
- FRONTIERE, N., RASKIN, C. D. & OWEN, J. M. 2017 Crksph – a conservative reproducing kernel smoothed particle hydrodynamics scheme. *J. Comput. Phys.* **332**, 160–209.
- GERMANO, M. 1992 Turbulence: the filtering approach. *J. Fluid Mech.* **238**, 325–336.
- GHOSAL, S. 1996 An analysis of numerical errors in large-eddy simulations of turbulence. *J. Comput. Phys.* **125** (1), 187–206.
- GINGOLD, R.A. & MONAGHAN, J.J. 1977 Smoothed particle hydrodynamics: theory and application to non-spherical stars. *Mon. Not. R. Astron. Soc.* **181**, 375—389.
- HALLER, G. 2015 Lagrangian coherent structures. *Annu. Rev. Fluid Mech.* **47**, 137–162.
- HARDY, R. J. 1982 Formulas for determining local properties in molecular-dynamics simulations: Shock waves. *J. Chem. Phys.* **76**, 622–628.
- HEISENBERG, W. 1948 Zur statistischen theorie der turbulenz. *Z. Physik* **124**, 628–657.
- HOPKINS, P.F. 2015 A new class of accurate, mesh-free hydrodynamic simulation methods. *Mon. Not. R. Astron. Soc.* **450**, 53.
- HOPKINS, P. F. 2016 Anisotropic diffusion in mesh-free numerical magnetohydrodynamics. *Mon. Not. R. Astron. Soc.* **466** (3), 3387–3405.
- IRVING, J. H. & KIRKWOOD, J. G. 1950 The statistical mechanical theory of transport processes. iv. the equations of hydrodynamics. *J. Chem. Phys.* **18** (6), 817–829.
- JAKOBSEN, H. A. 2014 *Chemical Reactor Modeling : Multiphase Reactive Flows*. Springer Cham.
- KING, J.R.C., LIND, S.J., ROGERS, B.D., STANSBY, P.K. & VACONDIO, R. 2023 Large eddy simulations of bubbly flows and breaking waves with smoothed particle hydrodynamics. *J. Fluid Mech.* **972**, A24.
- KOLMOGOROV, A. N. 1941 The local structure of turbulence in incompressible viscous fluid for very large reynolds numbers. *Dokl. Akad. Nauk SSSR* **30**, 4.
- KÜCHLER, CHRISTIAN, BEWLEY, GREGORY P. & BODENSCHATZ, EBERHARD 2023 Universal velocity statistics in decaying turbulence. *Phys. Rev. Lett.* **131**, 024001.
- LAI, X., LI, S., YAN, J., LIU, L. & ZHANG, A.-M. 2022 Multiphase large-eddy simulations of human cough jet development and expiratory droplet dispersion. *J. Fluid Mech.* **942**, A12.
- LAIZET, S. & LI, N. 2011 Incompact3d: A powerful tool to tackle turbulence problems with up to o(105) computational cores. *Int. J. Numer. Methods Fluids* **67** (11), 1735–1757.
- LIND, S.J., ROGERS, B.D. & STANSBY, P.K. 2020 Review of smoothed particle hydrodynamics: towards converged Lagrangian flow modelling. *Proc. R. Soc. A* **476**, 20190801.
- LUCY, L.B. 1977 A numerical approach to the testing of the fission hypothesis. *Astron. J.* **82**, 1013–1024.
- LUND, T.S. 2003 The use of explicit filters in large eddy simulation. *Comput. Math. Appl.* **46** (4), 603–616.
- MERINGOLO, D.D., LAURIA, A., ARISTODEMO, F. & FILIANOTI, P.F. 2023 Large eddy simulation within the smoothed particle hydrodynamics: Applications to multiphase flows. *Phys. Fluids* **35** (6), 063312.

- MONAGHAN, J.J. 2012 Smoothed Particle Hydrodynamics and Its Diverse Applications. *Annu. Rev. Fluid Mech.* **44**, 323–346.
- MOSER, R. D., HAERING, S. W. & YALLA, G. R. 2021 Statistical properties of subgrid-scale turbulence models. *Annu. Rev. Fluid Mech.* **53**, 255–286.
- MOURA, R. C., MENGALDO, G., PEIRÓ, J. & SHERWIN, S. J. 2017 On the eddy-resolving capability of high-order discontinuous galerkin approaches to implicit les / under-resolved dns of euler turbulence. *J. Comput. Phys.* **330**, 615–623.
- NICOUD, F., TODA, H. B., CABRIT, O., BOSE, S. & LEE, J. 2011 Using singular values to build a subgrid-scale model for large eddy simulations. *Phys. Fluids* **23**, 085106.
- OBUKHOV, A. M. 1941 On the distribution of energy in the spectrum of turbulent flow. *Dokl. Akad. Nauk SSSR* **32**, 22–24.
- OGER, G., MARRONE, S., LE TOUZÉ, D. & DE LEFFE, M. 2016 SPH accuracy improvement through the combination of a quasi-Lagrangian shifting transport velocity and consistent ALE formalisms. *J. Comput. Phys.* **313**, 76–98.
- OKRASCHEVSKI, M. 2024 Über den Zusammenhang von Large Eddy Simulation und Smoothed Particle Hydrodynamics. PhD thesis, Karlsruher Institut für Technologie (KIT).
- OKRASCHEVSKI, M., BUERKLE, N., KOCH, R. & BAUER, H.-J. 2021a Implicit molecular stresses in weakly compressible particle-based discretization methods for fluid flow. *Phys. Rev. E* **103**, 033304.
- OKRASCHEVSKI, M., BUERKLE, N., KOCH, R. & BAUER, H.-J. 2022 Smoothed particle hydrodynamics physically reconsidered: The relation to explicit large eddy simulation and the issue of particle duality. *Phys. Fluids* **34** (11), 115108.
- OKRASCHEVSKI, M., HOFFMANN, S., STICHLING, K., KOCH, R. & BAUER, H.-J. 2021b Fluid dynamics beyond the continuum: A physical perspective on large-eddy simulation. *Phys. Rev. Fluids* **6**, L102601.
- ONSAGER, L. 1945 The distribution of energy in turbulence. *Phys. Rev.* **68**, 281.
- PARK, N., YOO, J. Y. & CHOI, H. 2004 Toward improved consistency of a priori tests with a posteriori tests in large eddy simulation. *Phys. Fluids* **17** (1), 015103.
- PEREIRA, F. S., GRINSTEIN, F. F., ISRAEL, D. M., RAUENZAHN, R. & GIRIMAJI, S. S. 2021 Modeling and simulation of transitional taylor-green vortex flow with partially averaged navier-stokes equations. *Phys. Rev. Fluids* **6**, 054611.
- POSCH, H. A., HOOVER, W. G. & KUM, O. 1995 Steady-state shear flows via nonequilibrium molecular dynamics and smooth-particle applied mechanics. *Phys. Rev. E* **52**, 1711–1720.
- PRICE, D.J. 2012 Smoothed particle hydrodynamics and magnetohydrodynamics. *J. Comput. Phys.* **231**, 759–794.
- RENNEHAN, D. 2021 Mixing matters. *Mon. Not. R. Astron. Soc.* **506**, 2836–2852.
- REYNOLDS, O. 1895 IV. on the dynamical theory of incompressible viscous fluids and the determination of the criterion. *Philos. Trans. R. Soc. London, Ser. A* **186**, 123–164.
- SCHMITT, F. G. 2007 About Boussinesq’s turbulent viscosity hypothesis: historical remarks and a direct evaluation of its validity. *C. R. Mecanique* **335**, 617–627.
- SHADLOO, M.S., OGER, G. & TOUZE, D. LE 2016 Smoothed particle hydrodynamics method for fluid flows, towards industrial applications: Motivations, current state, and challenges. *Comput. Fluids* **136**, 11–34.
- SIGALOTTI, L., KLAPP, J. & GESTEIRA, M. 2021 The Mathematics of Smoothed Particle Hydrodynamics (SPH) Consistency. *Front. Appl. Math. Stat.* **7**.
- SILVIS, M. H., REMMERSWAAL, R. A. & VERSTAPPEN, R. 2017 Physical consistency of subgrid-scale models for large-eddy simulation of incompressible turbulent flows. *Phys. Fluids* **29** (1), 015105.
- SKRBEK, L. & STALP, S. R. 2000 On the decay of homogeneous isotropic turbulence. *Phys. Fluids* **12** (8), 1997–2019.
- SPRINGEL, V. 2010 Smoothed Particle Hydrodynamics in Astrophysics. *Annu. Rev. Astron. Astrophys.* **48**, 391–430.
- TAYLOR, G. I. & GREEN, A. E. 1937 Mechanism of the production of small eddies from large ones. *Philos. Trans. R. Soc. London, Ser. A* **158**, 499–521.
- VIGNJEVIC, R., DEVUYST, T. & CAMPBELL, J. 2021 The nonlocal, local and mixed forms of the SPH method. *Comput. Methods Appl. Mech. Eng.* **387**, 114164.
- VILA, J.P. 1999 On particle weighted methods and smooth particle hydrodynamics. *Math. Models Methods Appl. Sci.* **09** (02), 161–209.
- VOGELSBERGER, M., SIJACKI, D., KEREŠ, D., SPRINGEL, V. & HERNQUIST, L. 2012 Moving mesh cosmology: numerical techniques and global statistics. *Mon. Not. R. Astron. Soc.* **425** (4), 3024–3057.

- VREMAN, B., GEURTS, B. & KUERTEN, H. 1994 Realizability conditions for the turbulent stress tensor in large-eddy simulation. *J. Fluid Mech.* **278**, 351–362.
- YAO, W.-W., ZHOU, X.-P. & QIAN, Q.-H. 2022 From statistical mechanics to nonlocal theory. *Acta. Mech.* **233**, 869–887.
- YE, T., PAN, D., HUANG, C. & LIU, M. 2019 Smoothed particle hydrodynamics (SPH) for complex fluid flows: Recent developments in methodology and applications. *Phys. Fluids* **31**, 011301.
- ZHU, Q., HERNQUIST, L. & LI, Y. 2015 Numerical convergence in smoothed particle hydrodynamics. *Astrophys. J.* **800**, 6.